Flexible Metal Halide Perovskite Photodetector Arrays via Photolithography and Dry Lift-Off Patterning

Benzheng Xia, Min Tu, Bapi Pradhan, Frederik Ceyssens, Max Lutz Tietze, Víctor Rubio-Giménez, Nathalie Wauteraerts, Yujie Gao, Michael Kraft, Julian A. Steele, Elke Debroye, Johan Hofkens, and Rob Ameloot**

Metal halide perovskites draw increasing attention as photodetector materials due to their strong visible light absorption and resulting photocurrent. The development of efficient fabrication routes to realize high-resolution perovskite pixel arrays is critical to enable practical devices. Herein, a dry lift-off process to fabricate methylammonium lead iodide ($MAPbI_3$) pixels on different substrates is reported, with a resolution down to 5 µm. Accordingly, 8 × 10 photodetector arrays are fabricated on both glass and flexible polyethylene terephthalate (PET). These arrays show a sensitive photoresponse over a broad wavelength range from 320 to 760 nm. Moreover, when encapsulated by a Parylene-C overlayer, the photodetector arrays on glass substrate show remarkable air stability, without noticeable performance loss after 10 days in ambient air, and the flexible photodetector arrays on PET substrate show excellent bending tolerance, retaining nearly 95% of the response after 170 bending cycles.

1. Introduction

With the emergence of deformable electronics, the demand for flexible photodetectors is growing.[1–3] Organic, inorganic, and hybrid semiconductors have been intensively studied and can exhibit outstanding performances in terms of stability and detectivity.[4–6] Among them, metal halide perovskite materials have drawn tremendous attention because of their promising power conversion efficiency and charge transport characteristics.[7–10] To achieve the integration of metal halide perovskites into electronic and optoelectronic devices, a microfabrication process flow including an efficient patterning method is required.[11–13] However, current approaches to achieve high-resolution perovskite patterns have shortcomings (**Table 1**). The most explored technique in manufacturing pixel arrays, thermal evaporation through a fine shadow mask, is costly due to the need for high-temperature and extreme vacuum conditions.[14,15] Moreover, some strategies to improve film quality, such as additive and solvent engineering and thermal treatment, are difficult to combine with the evaporation technique. Solution processing under mild conditions, for instance, through inkjet printing or imprinting, is a low-cost alternative route toward perovskite pixels. However, although inkjet-printed features can be as small as a few micrometers,[16–18] controlling the shape and landing position of the printed droplets is challenging.[19] The perovskite patterns made by imprinting are continuous, which results in crosstalk between neighboring devices.[20,21]

In microelectronics fabrication, photolithography is the standard method to enable reproducible and high-resolution patterning. For instance, in lift-off patterning, a blanket film of the target material is deposited on a substrate covered with a single-use mask, typically a patterned photoresist layer. The pattern is

B. Xia, M. Tu, F. Ceyssens, M. L. Tietze, V. Rubio-Giménez, N. Wauteraerts, Y. Gao, J. A. Steele, R. Ameloot
Centre for Membrane Separations, Adsorption, Catalysis, and Spectroscopy (cMACS)
KU Leuven
3001 Leuven, Belgium
E-mail: rob.ameloot@kuleuven.be

M. Tu
2020 X-Lab
Shanghai Institute of Microsystem and Information Technology
Chinese Academy of Sciences
Shanghai, China
E-mail: min.tu@mail.sim.ac.cn

M. Tu
State Key Laboratory of Transducer Technology
Shanghai Institute of Microsystem and Information Technology
Chinese Academy of Sciences
Shanghai, China

B. Pradhan, E. Debroye, J. Hofkens
Molecular Visualization and Photonics
KU Leuven
3001 Leuven, Belgium

F. Ceyssens, M. Kraft
Micro- and Nano Systems (MNS)
KU Leuven
3001 Leuven, Belgium

J. Hofkens
Department Bonn
Max Planck Institute for Polymer Research
Ackermannweg 10, 55128 Mainz, Germany

Table 1. Comparison of perovskite patterning methods.

Method	Solution processing	Ambient conditions	Mask needed	Developer needed	Individually addressable pixels	Ref.
Thermal evaporation	N[a)]	N	Y	N	Y	[14,15]
Inkjet printing	Y[b)]	Y	N	N	Y	[16-18]
Imprinting	Y	Y	Y	N	N	[20,21]
Wet lift-off (photolithography)	Y	Y	Y	Y	Y	[22-24]
Dry lift-off (photolithography)	Y	Y	Y	N	Y	[26,28] & this work

[a)]No; [b)]Yes.

generated upon stripping the mask, leaving the target material only where it is in direct contact with the substrate. However, photolithographic patterning of perovskite materials is nontrivial due to their instability in the polar solvents and additives that make up photoresist developers and strippers. Therefore, to achieve the lithographic fabrication of perovskite patterns, the challenge is to find developer and stripper solutions that are orthogonal to perovskites.[22–24] Dry lift-off is an alternative process in which solvents are avoided entirely by mechanically stripping the mask. "Parylenes" are a group of polymers consisting of poly-para-xylylene and deposited through chemical vapor deposition (CVD). As the substrate can remain close to room temperature during deposition, Parylene coating is compatible with temperature-sensitive materials.[25] In addition, Parylene films are chemically inert and have mechanical properties that enable them to be peeled off even at low thicknesses. Patterning through Parylene dry lift-off has been reported for a range of target materials deposited either via solution processing or vacuum evaporation, including biological materials, as well as perovskite films and quantum dots.[26–28] In addition, because of their flexibility, mechanical strength, and barrier properties, Parylene films have been used both as an overlayer and a substrate in ultrathin devices.[29–31]

In this work, a dry lift-off process using Parylene-C was developed to fabricate high-resolution pixels of the metal halide perovskite $MAPbI_3$. Photodetector arrays consisting of 8×10 pixels were fabricated on glass and flexible PET substrates to realize visible light detection and imaging. The photodetectors exhibited good responsivity and reversibility and a broadband photoresponse. The imaging capability of the photodetector arrays was demonstrated through a masking approach. When encapsulated by a Parylene-C overlayer, the photodetector arrays showed remarkable bending tolerance and stability in air.

2. Results and Discussion

Scheme 1 shows the dry lift-off fabrication of $MAPbI_3$ pixels. A Teflon layer was first deposited to lower the adhesion of the Parylene-C film to the substrate, thus enabling complete peel-off.[32,33] Afterward, a Parylene-C film (2 μm) and a Mo layer (10 nm) were deposited. The Mo layer was patterned through photolithography and acid etching. The patterned Mo layer serves as a hard mask to pattern the Parylene-C layer via reactive ion etching (RIE) using mixed SF_6 and O_2 plasma. As a photoresist mask would be etched as well under these RIE conditions, it would have to be very thick. Instead, a Mo hard mask can be much thinner, which facilitates high-precision patterning of the Parylene-C layer.[34] After RIE, a blanket perovskite was deposited on the patterned surface by spin coating of a precursor solution, followed by annealing at 130 °C for 1 min. Finally, the Parylene-C film was peeled off to complete the perovskite pixel array. **Figure 1** shows the scanning electron microscopy (SEM) images of 5 and 10 μm $MAPbI_3$ dot patterns on Teflon-modified glass, Si, and flexible PET substrates. The crystallinity of the perovskite film was verified by X-ray diffraction. The resulting diffractogram can be fitted to a tetragonal β-$MAPbI_3$ phase exhibiting a preferred (110) out-of-plane orientation, together with a small fraction of unreacted PbI_2 (Figure S4a, Supporting Information).[35,36] The absence of $MAPbI_3$ residue in between the dots validates the successful application of the dry lift-off process. The pattern edges are not perfectly circular, presumably due to the volume reduction of the precursor solution in the Parylene-C pattern during solvent evaporation and annealing. If required, an even higher precision might be achievable through the combination of the dry lift-off strategy with more advanced deposition approaches.[26,37,38]

To construct a photodetector array, dry lift-off patterning was combined with the deposition of a planar electrode architecture that enables the electrical readout of each perovskite pixel. Each of the 8×10 pixels in the planar array design has an active area of $600 \times 600\ \mu m^2$ and can be addressed through a pair of Au interdigitated electrodes (IDEs) with a 20 μm line width and line spacing (Scheme S1, Supporting Information). The electrodes were fabricated on glass and PET, and, through precise alignment and dry lift-off, each pixel was coated with perovskite (**Figure 2**a and Figure S1–S3, Supporting Information). The resulting $MAPbI_3$ film had a thickness of ≈500 nm (Figure S3, Supporting Information) and the characteristic fiber-like structure (Figure S2d, Supporting Information).

For wavelengths ranging from 320 to 760 nm, the photoresponse of individual pixels was studied by current–voltage (I–V) measurements. All I–V curves, including those recorded in the absence of light, were nonlinear, similar to other reports on $MAPbI_3$.[39,40] Although symmetrical IDEs were used, the I–V curves showed asymmetric behavior (Figure 2b), possibly due to the formation of a Schottky contact between $MAPbI_3$ and the Au electrodes, which is sensitive to the interfacial state of $MAPbI_3$/Au.[40,41] The device responded to the tested wide wavelength range (Figure S5, Supporting Information), even for power

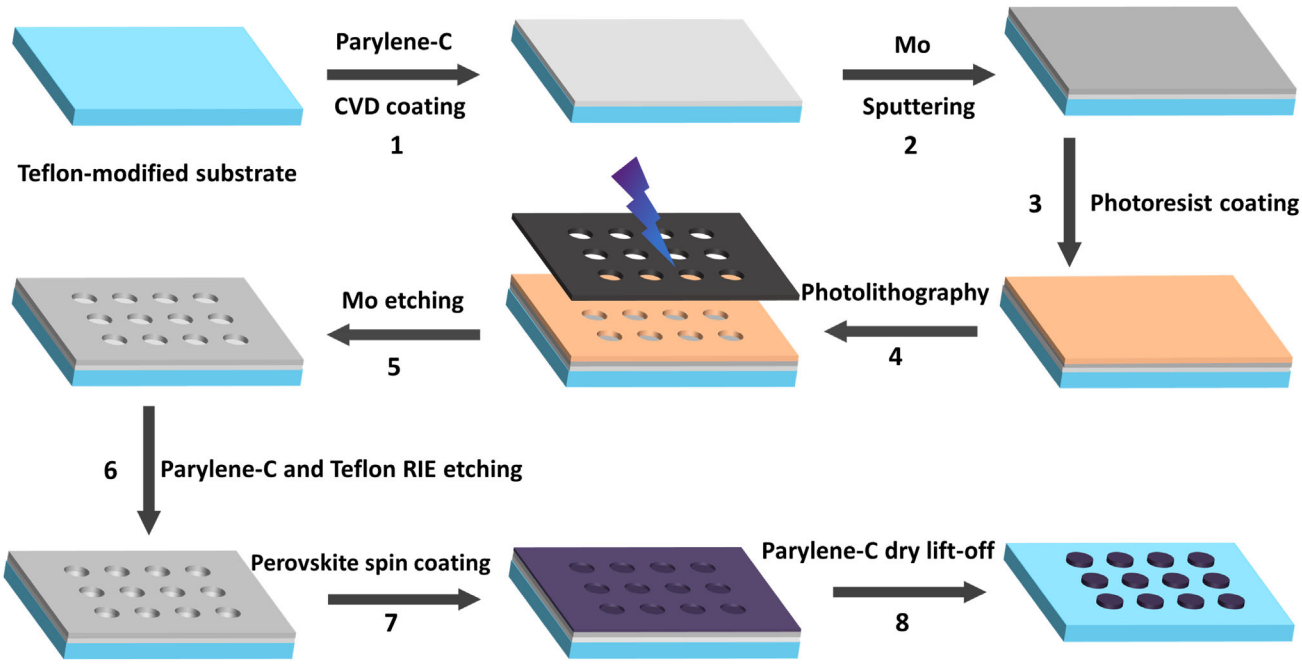

Scheme 1. Dry lift-off fabrication of $MAPbI_3$ pixels. A Teflon layer was first deposited by spin coating. Next, a 2 μm Parylene-C film was deposited (step 1). In step 2, a 10 nm molybdenum (Mo) layer was sputtered on the Parylene-C layer, followed by photoresist spin coating (step 3), photolithography (step 4), and wet etching of the Mo layer (step 5). In step 6, the resulting Mo pattern served as a hard mask to pattern the Parylene-C and Teflon layers by RIE. In step 7, the MAPbI3 layer was spin coated and annealed. The MAPbI3 pixels were generated by peeling off the patterned Parylene-C film (step 8).

densities as low as 5–100 μW cm^{-2}, although the response dropped off steeply at 320 nm. The photocurrent ($I_{ph} = I_{light} - I_{dark}$) shows a nearly linear relationship with the light intensity ranging from 20 to 100 μW cm^{-2} (Figure 2c and S5a, Supporting Information). The specific detectivity (D^*), one of the key figures of merit, describes the smallest detectable signal of the photodetector.[42] Assuming that the shot noise from dark current is the major source of noise, D^* was calculated as

$$D^* = \frac{R}{\sqrt[2]{2q\left(\frac{I_{dark}}{A}\right)}} \quad (1)$$

where the responsivity (R) was defined as

$$R = \frac{I_{ph}}{PA} \quad (2)$$

with I_{ph} as the photocurrent, P the illumination power density, and A the illuminated area. As shown in Figure 2c, the highest D^* value reaches 7.1×10^{10} Jones under 405 nm wavelength irradiation with an intensity of 20 μW cm^{-2}. The photocurrent was reversible for different light intensities (Figure 2d). The response time (photocurrent increases from 10% to 90% of the maximum value) and recovery time (photocurrent decreases from 90% to 10% of the maximum value) were measured to be 13 and 21 ms, respectively (Figure 2e). Although the performance of the photodetectors in this work is comparable with others based on $MAPbI_3$ films (Table S1, Supporting Information), the photocurrent and response speed are limited by the polycrystalline film and planar device structure. The $MAPbI_3$ films exhibit a fiber-like morphology, as commonly observed when depositing films through spin coating from DMF or DMSO solution.[43] Although the preferred (110) orientation and relatively large grain size are beneficial to improving carrier transport,[44] the incomplete coverage and high defect density of the resulting films lead to shorter carrier diffusion distances and a lower performance compared with single-crystal photodetectors.[45,46] In addition, compared with a vertical "sandwich" photodetector, the long channel distance of the planar IDEs decreases the response speed.[47] However, from the perspective of fabrication, the planar structure is a more practical route to large-area photodetector arrays due to the fewer patterning steps.[48] Therefore, it would be worthwhile to investigate planar photodetectors based on IDEs with a shorter channel distance and coated with uniform perovskite films with preferred orientation.[37,49,50]

The dry lift-off strategy was also applied to fabricate a flexible photodetector on PET. The fabrication process was the same as on glass, except that a 2 μm Parylene-C film was deposited on top of the perovskite pattern as a protective layer in the last step. A specific single-pixel device was designed to test the bending tolerance (**Figure 3**a and S6, Supporting Information). The I–V curves under white light illumination (1.4 mW cm^{-2}) show a similar transport behavior for different bending strains (ε),[51] indicating that the film quality is maintained under bending conditions (Figure 3b). Despite a decrease in light current (from 380 to 300 nA) at a bending strain of 0.4%, the flexible device showed a similar light current under even more severe bending (bending

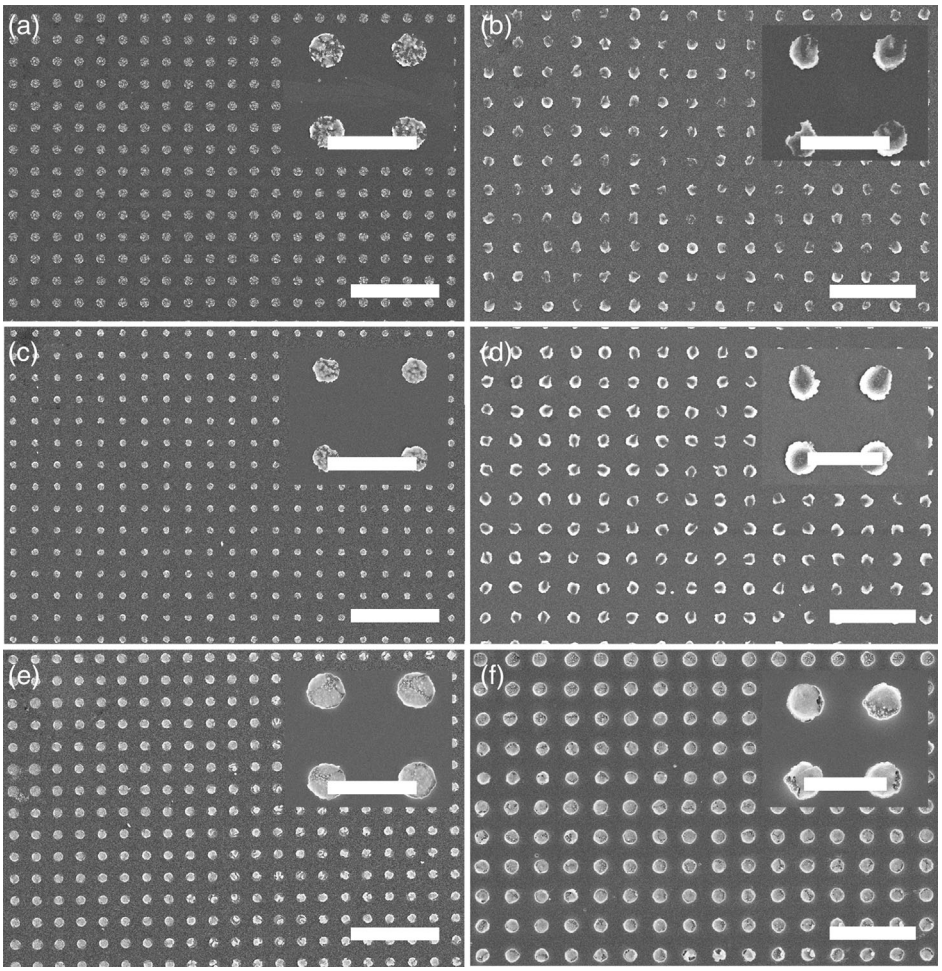

Figure 1. $MAPbI_3$ dot patterns. 10 μm-diameter circles on a) Si, c) glass, and e) PET. Scale bar: 120 μm, inset: 30 μm. 5 μm-diameter circles on b) Si, d) glass, and f) PET. Scale bar: 30 μm, inset: 10 μm.

strain of 1.7%), and a repeatable on/off response was maintained in both the flat and bent state (Figure 3c). While the reference devices without Parylene-C encapsulation degrade after ten bending cycles (Figure 3d), the ones with a Parylene-C protective coating maintain 95% of the light current after 170 bending cycles, indicating a significantly improved bending tolerance. In addition, the Parylene-C overlayer also dramatically improves the air stability of $MAPbI_3$-based photodetectors, with no obvious loss of light current in ambient air after 10 days (Figure 3e). In contrast, without Parylene-C encapsulation, the light current dropped by nearly 90% after 24 h (Figure 3e and Figure S7c, Supporting Information), together with a color change from black to yellow–gray, as previously reported for perovskite degradation.[36,52,53]

The imaging functionality of the photodetector array on glass was evaluated by illuminating the 8×10 array through a mask possessing a single hole with the size of $1 \times 1\ mm^2$ (Figure S8a, Supporting Information). The current of all pixels in the array was measured, resulting in a photocurrent response for the pixel aligned with the hole and a dark current background measurement for all others. The measurement was repeated for different mask positions, each time aligning the hole with another pixel. The resulting trace, consisting of the photocurrent recorded for all illuminated pixels, illustrates the potential of the array in imaging. The average photocurrent of 22 illuminated pixels was 128 nA, with extremes at 60 and 224 nA (**Figure 4**b and Figure S8b, Supporting Information). This spread in the photocurrent response might be caused by the nonuniformity of the one-step spin-coated film, which exhibits fiber-like morphology. The morphology of the resulting film is crucially determined by the seed crystals in the precursor solution, which can grow to a large size and prevent further nucleation due to the slow evaporation of the DMF solvent during spin coating.[43] Therefore, despite the added complexity, extra treatments are more beneficial to form a uniform film covering the entire substrate. Examples of such additional treatments are antisolvent washing or two-step coating, which can induce rapid nuclearization and high density of seed crystals.[43] In addition, the uniformity of spin-coated films is unfavorable, which limits its application in large-area devices.[54] Methods used in large-scale solution processing, such as blade coating, roll printing, etc., are worth exploring to evaluate their compatibility with the Parylene-C patterning method.[37]

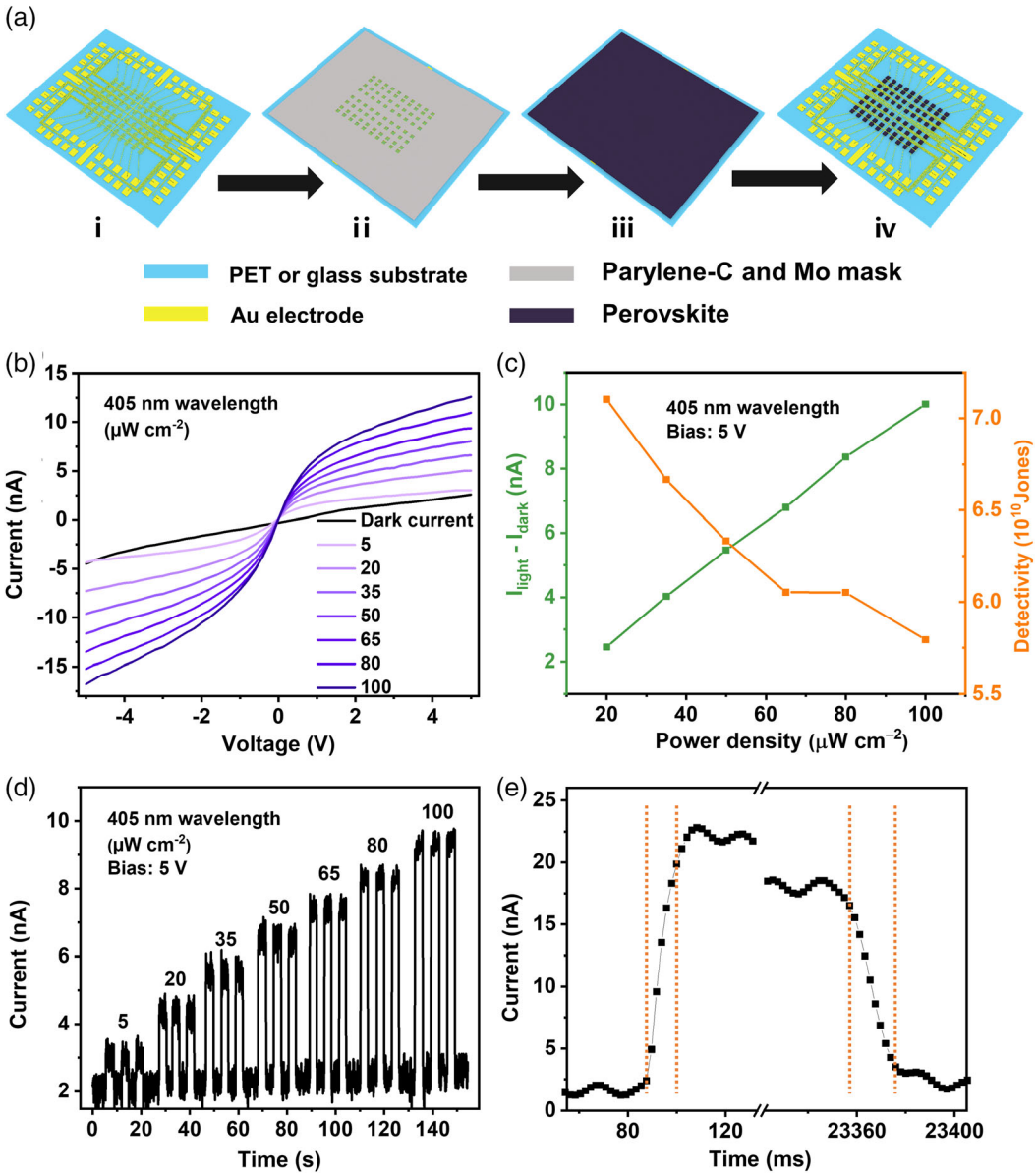

Figure 2. $MAPbI_3$ photodetector array fabrication and testing. a) Photodetector fabrication on glass or PET. (i) Au electrode deposition. (ii) Parylene-C mask formation, (iii) $MAPbI_3$ perovskite film deposition, (iv) perovskite photodetector array obtained after Parylene-C dry lift-off. b) *I–V* curves of an individual pixel under illumination ($\lambda = 405$ nm) with power densities ranging from 0 to 100 μW cm^{-2}. c) The dependence of the photocurrent and detectivity on power densities. d) Repeatable on/off photoresponse at different power densities and a fixed bias voltage of 5 V. e) The response and recovery time of an individual pixel measured under 1.4 mW cm^{-2} white light illumination.

3. Conclusion

In conclusion, Parylene-C dry lift-off patterning was explored on PET, Si, and glass substrates, aided by a Teflon modification strategy. The fabrication of perovskite pixels with a resolution down to 5 μm on both rigid and flexible substrates via the dry lift-off route was achieved. This straightforward method was demonstrated to be compatible with device fabrication. $MAPbI_3$-based planar photodetector arrays were fabricated with a response to light ranging from 320 to 760 nm and a detectivity of 7.1×10^{10} Jones for 405 nm irradiation at 20 μW cm^{-2}. Beneficial from the clear boundaries of each pixel, there is no crosstalk among adjacent photodetectors, which is promising for imaging applications. In addition, Parylene-C protective layers were shown to enable remarkable air stability and bending tolerance.

4. Experimental Section

Materials: All the chemicals were ordered from commercial suppliers and were used without further purification. PbI_2 (99.999% trace metals basis) and dimethylformamide (DMF, anhydrous, 99.8%) were purchased from Sigma-Aldrich. Methylammonium iodide (MAI, >99.99%) was purchased from Greatcell Solar Materials. The ma-N 1420 photoresist was purchased from Micro resist technology. Glass slides (550 μm thick) were purchased from

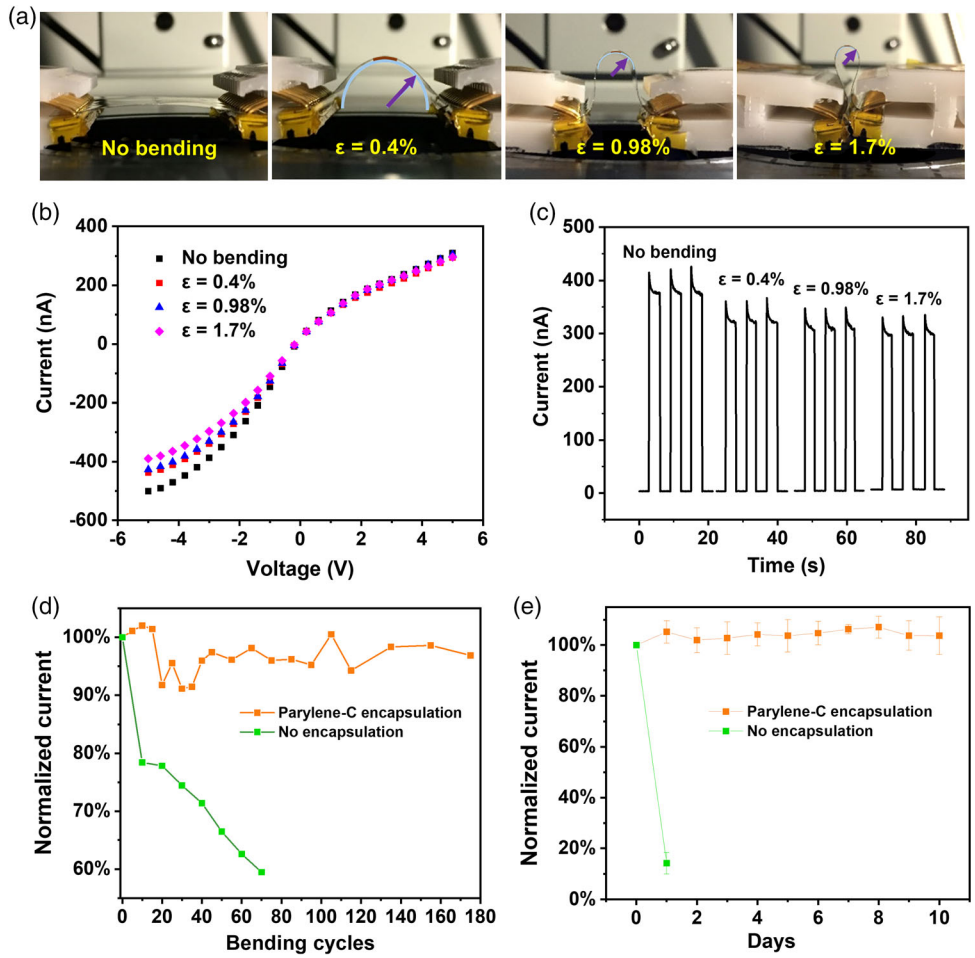

Figure 3. Bending tolerance of devices on PET and air stability of devices on glass. All measurements were carried out under 1.4 mW cm^{-2} white light illumination. a) Single-pixel test devices under different bending strains. b) *I–V* curves and c) repeatable on/off photoresponse to white light under different bending strains with a bias voltage of 5 V. d) Bending tolerance test with and without Parylene-C encapsulation. The device was bent for the specified number of cycles and subsequently tested while flat. e) Air stability of photodetectors on glass with and without Parylene-C encapsulation. The standard deviations are calculated from five different devices. The light current was extracted for a bias voltage of 5 V.

Drix NV. Si wafers were purchased from Si-Mat. Polyethylene terephthalate (PET, 75 µm thickness) was purchased from goodfellow.com. DuPont AF was purchased from Dupont (Wilmington, DE, USA). Fluorinert FC-40 was purchased from Sigma-Aldrich. Parylene-C was purchased from J&K (92%).

Fabrication of Perovskite Pixel Array: All of the fabrication procedures were conducted in air in the KU Leuven Nanocenter cleanroom facility (Class 1000). The substrates (Si, glass, or PET) were cleaned by acetone and deionized (DI) water and dried by compressed airflow. The direct deposition of Parylene-C on these substrates would lead to strong adhesion, making it impossible to cleanly peel off the Parylene-C film. Therefore, a dilute Teflon solution (by mixing DuPont AF amorphous fluoroplastics solution and Perfluoro-compound FC-40 in a volumetric ratio of 1:10) was spin coated on the substrate at 3 k RPM for 30 s, followed by baking at 100 °C for 5 min. The dilution ratio of the Teflon solution was fine tuned to ensure appropriate adhesion between the deposited Parylene-C coating and the substrates. Then, 2 µm-thick Parylene-C was deposited via CVD (plasma Parylene systems, PPS). The thickness was controlled through the quantity of Parylene-C. The raw Parylene-C dimer was vaporized at 140 °C and cracked to Parylene-C monomers at 720 °C, which entered into the coating chamber and polymerized on the substrate at nearly room temperature. Next, 10 nm Mo was deposited via magnetron sputtering (2×10^{-3} mbar pressure, 70 sccm Ar flow, radio frequency [RF] power of 200 W, and 30 s deposition time). After that, a negative photoresist ma-N 1420 was spin coated at 3 K RPM for 30 s and baked on a hotplate at 100 °C for 2 min. After 300 mJ cm^{-2} 312 nm UV light exposure, while covered by a photomask, the photoresist was developed in ma-D 533/S developer. The Mo layer was etched for 30 s using the Transene type-A aluminum etchant consisting of H_3PO_4, HNO_3, CH_3COOH, and H_2O in a 80:5:5:10 volumetric ratio. With the Mo mask in place, the Parylene-C layer was etched by mixed SF_6 and O_2 plasma (10 sccm SF_6: 30 sccm O_2) with an etching power of 110 W and etching pressure of 20 mTorr. Stoichiometric quantities of MAI (39.8 mg, 0.25 mmol) and PbI_2 (115.2 mg, 0.25 mmol) were dissolved in DMF (500 µL) and stirred overnight at room temperature to form a 0.5 M $MAPbI_3$ solution. This solution was spin coated (1 k RPM, 30 s) on the patterned substrate and annealed on a hotplate at 130 °C for 1 min. In the last step, Parylene-C pattern was peeled off with tweezers to form the pixel array.

Fabrication of Gold Electrodes: The electrode was fabricated via the photoresist lift-off method, as shown in Scheme S1, Supporting Information. First, the substrate (PET or glass) was cleaned by acetone and DI water and dried by compressed airflow. A negative photoresist ma-N 1420 was spin coated on the substrate at 3000 RPM for 30 s and baked at 100 °C for 2 min on a hotplate. Then, the photoresist layer was patterned with a photolithography procedure (UV exposure at 300 mJ cm^{-2}) and developed in ma-D 533/S developer. After that, ≈10 nm titanium and ≈70 nm gold were sequentially deposited on the substrate by magnetron sputtering.

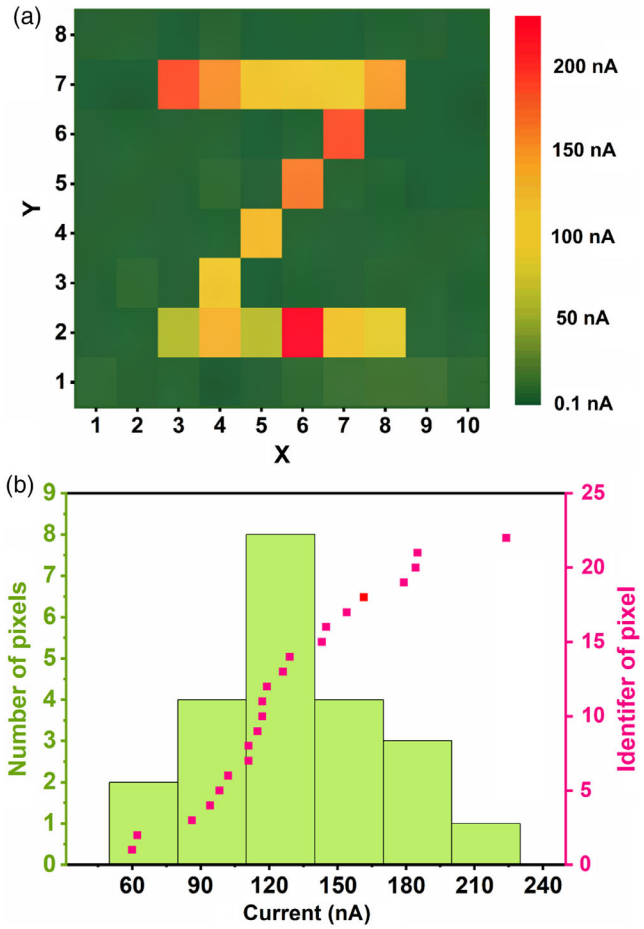

Figure 4. Photoresponse of the detector array on glass under 1.4 mW cm^{-2} white light illumination and a bias voltage of 5 V. a) Dark and photocurrent mapping of the 8 × 10 array. The imaging test was conducted by illuminating individual pixels sequentially via a shadow mask. b) Photoresponse distribution for 22 pixels. The histogram indicates the number of pixels in each range. The red scatter plot gives the photocurrent for each pixel.

The sputtering parameters were 2×10^{-3} mbar pressure, and 70 sccm Ar flow; the RF powers for Ti and Au sputtering were 200 and 80 W, respectively. Finally, the substrate was rinsed with acetone to lift off the photoresist. The substrate was cleaned with DI water and dried with compressed air.

Fabrication of Photodetector Array: The photodetector array fabrication was similar to the high-resolution pixel array fabrication. To etch the Parylene-C above the interdigital electrode precisely, an alignment step was needed (Figure 2a). The $MAPBI_3$ precursor solution was spin coated and annealed at 130 °C for 1 min. Patterning was conducted by peeling off the Parylene-C mask.

Characterizations and Measurements: The perovskite arrays were imaged by SEM (JEOL JSM-6010LV). The crystallinity of the $MAPbI_3$ film was analyzed with a Malvern PANalytical Empyrean diffractometer in Bragg–Brentano geometry (gonio mode) using a Cu anode operating at 45 kV and 40 mA and PIXcel3D solid-state detector (step size 0.0525°, counting time 1000 s) within a 5°–60° range. Structural refinement of X-ray scattering patterns: The full scattering patterns were modeled using the Le Bail method in Fullprof.[55] The recorded pattern was indexed to an tetragonal (I4cm) β-phase perovskite and the preferential orientation was taken into account via the March–Dollase's approach.[56] The best fit was realized when a strong (110) out-of-plane orientation was adopted. The $MAPbI_3$ film was produced by spin coating 0.5 M $MAPbI_3$ precursor solution on UV–O_3-treated Si substrate and annealed at 130 °C for 1 min. UV–vis reflectance spectra were recorded on a Perkin Elmer Lambda 950 UV–VIS–NIR. The $MAPbI_3$ film was produced by spin coating 0.5 M $MAPbI_3$ precursor solution on UV–O_3-treated quartz substrate and annealed at 130 °C for 1 min. Electrical measurements of the photoresponse were carried out using a Keithley 2614B, 2-channel source measurement unit. A 3M 2 × 14 pins IC test clip was used to contact the electrodes of the photodetector arrays. A fluorescence spectrometer (FLS980) was used as a light source with controllable wavelength and intensity. To test the bending tolerance of the flexible photodetector pixel, the specifically designed devices were fixed on the stage of the microscopy under white light illumination (tungsten lamp, FluoView FV1000 confocal microscope, Olympus). The bending line ran through the center of the pixel. To determine the different bending radii, the two test clamps were fixed on the microscope stage at defined distances. The length of the device without bending (28 mm) was used as a reference to calculate the bending radii from the pictures. The bending strain (ε) is approximated by the equation $\varepsilon = d_s/2R_c$, where d_s is the thickness of the substrate (75 µm) and R_c is the bending radius. White light illumination from the FluoView FV1000 confocal microscope was also used to test the stability and imaging function. The thickness of the photodetector pixel was measured via contact profilometry (Bruker Dektak XT).

Supporting Information

Supporting Information is available from the Wiley Online Library or from the author.

Acknowledgements

This project received funding from the European Research Council (ERC) under the European Union's Horizon 2020 research and innovation program (grant agreement no. 716472, acronym VAPORE). The Research Foundation Flanders (FWO) is acknowledged for funding the research project, G85720N, S002019N, 1514220N, G.0B39.15, G.0B49.15, G098319N, and ZW15_09-GOH6316. B.P., M.L.T., V.R.-G., N.W., J.A.S., and E.D. thank FWO for the fellowships 1275521N, 12ZK720N, 12Z6520N, 1SB7921N, 12Y7221N, and 12O3719N, respectively. J.H. thanks the Flemish government for long-term structural funding Methusalem (CASAS2, Meth/15/04) and the MPI for financial support as an MPI fellow. K.U. Leuven is acknowledged for funding in the research project C32/18/056. B.X. and Y.G. thank the China Scholarship Council (CSC) for the fellowships 201704910802 and 201806650002, respectively. All authors have given approval to the final version of the manuscript.

[1] L. Gu, S. Poddar, Y. Lin, Z. Long, D. Zhang, Q. Zhang, L. Shu, X. Qiu, M. Kam, A. Javey, Z. Fan, *Nature* **2020**, *581*, 278.

[2] E. O. Polat, G. Mercier, I. Nikitskiy, E. Puma, T. Galan, S. Gupta, M. Montagut, J. J. Piqueras, M. Bouwens, T. Durduran, G. Konstantatos, S. Goossens, F. Koppens, *Sci. Adv.* **2019**, *5*, eaaw7846.

[3] L. Clinckemalie, D. Valli, M. B. J. Roeffaers, J. Hofkens, B. Pradhan, E. Debroye, *ACS Energy Lett.* **2021**, *6*, 1290.

[4] J. Chen, W. Ouyang, W. Yang, J. He, X. Fang, *Adv. Funct. Mater.* **2020**, *30*, 1909909.

[5] J. Feng, C. Gong, H. Gao, W. Wen, Y. Gong, X. Jiang, B. Zhang, Y. Wu, Y. Wu, H. Fu, L. Jiang, X. Zhang, *Nat. Electron.* **2018**, *1*, 404.

[6] F. P. García de Arquer, A. Armin, P. Meredith, E. H. Sargent, *Nat. Rev. Mater.* **2017**, *2*, 16100.

[7] A. Al-Ashouri, E. Köhnen, B. Li, A. Magomedov, H. Hempel, P. Caprioglio, J. A. Márquez, A. B. M. Vilches, E. Kasparavicius, J. A. Smith, N. Phung, D. Menzel, M. Grischek, L. Kegelmann, D. Skroblin, C. Gollwitzer, T. Malinauskas, M. Jo, R. Schlatmann, M. Topic, L. Korte, A. Abate, B. Stannowski, D. Neher, M. Stolterfoht, T. Unold, V. Getautis, S. Albrecht, *Science* **2020**, *370*, 1300.

[8] T. Wu, W. Pisula, M. Y. A. Rashid, P. Gao, *Adv. Electron. Mater.* **2019**, *5*, 1900444.

[9] W. Li, A. Stroppa, Z.-M. Wang, S. Gao, *Hybrid Organic-Inorganic Perovskites*, John Wiley & Sons, Hoboken, NJ **2020**.

[10] W. Li, Z. Wang, F. Deschler, S. Gao, R. H. Friend, A. K. Cheetham, *Nat. Rev. Mater.* **2017**, *2*, 16099.

[11] B. Jeong, H. Han, C. Park, *Adv. Mater.* **2020**, *32*, 2000597.

[12] W. Liu, H. Zhou, G. Chen, *Cryst. Growth Des.* **2020**, *20*, 2803.

[13] Y. Zou, L. Cai, T. Song, B. Sun, *Small Sci.* **2020**, 2000050.

[14] A. Daus, C. Roldán-Carmona, K. Domanski, S. Knobelspies, G. Cantarella, C. Vogt, M. Grätzel, M. K. Nazeeruddin, G. Tröster, *Adv. Mater.* **2018**, *30*, 1707412.

[15] G. Kim, S. An, S.-K. Hyeong, S.-K. Lee, M. Kim, N. Shin, *Chem. Mater.* **2019**, *31*, 8212.

[16] L. Shi, L. Meng, F. Jiang, Y. Ge, F. Li, X. Wu, H. Zhong, *Adv. Funct. Mater.* **2019**, *29*, 1903648.

[17] Z. Gu, Z. Zhou, Z. Huang, K. Wang, Z. Cai, X. Hu, L. Li, M. Li, Y. S. Zhao, Y. Song, *Adv. Mater.* **2020**, *32*, 1908006.

[18] M. Zhu, Y. Duan, N. Liu, H. Li, J. Li, P. Du, Z. Tan, G. Niu, L. Gao, Y. Huang, Z. Yin, J. Tang, *Adv. Funct. Mater.* **2019**, *29*, 1903294.

[19] X. Peng, J. Yuan, S. Shen, M. Gao, A. S. R. Chesman, H. Yin, J. Cheng, Q. Zhang, D. Angmo, *Adv. Funct. Mater.* **2017**, *27*, 1703704.

[20] S. V. Makarov, V. Milichko, E. V. Ushakova, M. Omelyanovich, A. Cerdan Pasaran, R. Haroldson, B. Balachandran, H. Wang, W. Hu, Y. S. Kivshar, A. A. Zakhidov, *ACS Photonics* **2017**, *4*, 728.

[21] N. Pourdavoud, S. Wang, A. Mayer, T. Hu, Y. Chen, A. Marianovich, W. Kowalsky, R. Heiderhoff, H.-C. Scheer, T. Riedl, *Adv. Mater.* **2017**, *29*, 1605003.

[22] J. Harwell, J. Burch, A. Fikouras, M. C. Gather, A. Di Falco, I. D. W. Samuel, *ACS Nano* **2019**, *13*, 3823.

[23] C. H. Lin, Q. Zeng, E. Lafalce, S. Yu, M. J. Smith, Y. J. Yoon, Y. Chang, Y. Jiang, Z. Lin, Z. V. Vardeny, V. V. Tsukruk, *Adv. Opt. Mater.* **2018**, *6*, 1800474.

[24] W. Mei, Z. Zhang, A. Zhang, D. Li, X. Zhang, H. Wang, Z. Chen, Y. Li, X. Li, X. Xu, *Nano Res.* **2020**, *13*, 2485.

[25] E. Meng, Yu-Chong Tai, in *18th IEEE Int. Conf. on Micro Electro Mechanical Systems, 2005. MEMS 2005*, IEEE, Miami Beach, FL **2005**, p. 568.

[26] C. Zou, C. Chang, D. Sun, K. F. Böhringer, L. Y. Lin, *Nano Lett.* **2020**, *20*, 3710.

[27] K. Kuribayashi, Y. Hiratsuka, T. Yamamura, S. Takeuchi, in *2007 IEEE 20th Int. Conf. on Micro Electro Mechanical Systems (MEMS)*, IEEE, Hyogo, Japan **2007**, p. 501.

[28] A. Chanana, X. Liu, C. Zhang, Z. V. Vardeny, A. Nahata, *Sci. Adv.* **2018**, *4*, 7353.

[29] W. Wu, X. Han, J. Li, X. Wang, Y. Zhang, Z. Huo, Q. Chen, X. Sun, Z. Xu, Y. Tan, C. Pan, A. Pan, *Adv. Mater.* **2021**, *33*, 2006006.

[30] H. Jinno, K. Fukuda, X. Xu, S. Park, Y. Suzuki, M. Koizumi, T. Yokota, I. Osaka, K. Takimiya, T. Someya, *Nat. Energy* **2017**, *2*, 780.

[31] C. Keum, C. Murawski, E. Archer, S. Kwon, A. Mischok, M. C. Gather, *Nat. Commun.* **2020**, *11*, 6250.

[32] D. Witters, N. Vergauwe, S. Vermeir, F. Ceyssens, S. Liekens, R. Puers, J. Lammertyn, *Lab Chip* **2011**, *11*, 2790.

[33] D. Witters, K. Knez, F. Ceyssens, R. Puers, J. Lammertyn, *Lab Chip* **2013**, *13*, 2047.

[34] L. Zhang, Y. Liu, Z. Li, W. Wang, *Micromachines* **2018**, *9*, 162.

[35] C. C. Stoumpos, C. D. Malliakas, M. G. Kanatzidis, *Inorg. Chem.* **2013**, *52*, 9019.

[36] S. Bai, P. Da, C. Li, Z. Wang, Z. Yuan, F. Fu, M. Kawecki, X. Liu, N. Sakai, J. T.-W. Wang, S. Huettner, S. Buecheler, M. Fahlman, F. Gao, H. J. Snaith, *Nature* **2019**, *571*, 245.

[37] L. Lee, J. Baek, K. S. Park, Y.-E. Lee, N. K. Shrestha, M. M. Sung, *Nat. Commun.* **2017**, *8*, 15882.

[38] X. Wang, W. Li, J. Liao, D. Kuang, *Sol. RRL* **2019**, *3*, 1800294.

[39] W. Wang, Y. Ma, L. Qi, *Adv. Funct. Mater.* **2017**, *27*, 1603653.

[40] Y. Zhang, J. Du, X. Wu, G. Zhang, Y. Chu, D. Liu, Y. Zhao, Z. Liang, J. Huang, *ACS Appl. Mater. Interfaces* **2015**, *7*, 21634.

[41] W. Wu, X. Wang, X. Han, Z. Yang, G. Gao, Y. Zhang, J. Hu, Y. Tan, A. Pan, C. Pan, *Adv. Mater.* **2019**, *31*, 1805913.

[42] L. Dou, Y. (Micheal) Yang, J. You, Z. Hong, W.-H. Chang, G. Li, Y. Yang, *Nat. Commun.* **2014**, *5*, 5404.

[43] W. A. Dunlap-Shohl, Y. Zhou, N. P. Padture, D. B. Mitzi, *Chem. Rev.* **2019**, *119*, 3193.

[44] B. Zhang, M.-J. Zhang, S.-P. Pang, C.-S. Huang, Z.-M. Zhou, D. Wang, N. Wang, G.-L. Cui, *Adv. Mater. Interfaces* **2016**, *3*, 1600327.

[45] J. C. Hamil Jr., J. Schwartz, Y.-L. Loo, *ACS Energy Lett.* **2018**, *3*, 92.

[46] W. Deng, L. Huang, X. Xu, X. Zhang, X. Jin, S.-T. Lee, J. Jie, *Nano Lett.* **2017**, *17*, 2482.

[47] H. Wang, D. H. Kim, *Chem. Soc. Rev.* **2017**, *46*, 5204.

[48] Z. Lian, Q. Yan, Q. Lv, Y. Wang, L. Liu, L. Zhang, S. Pan, Q. Li, L. Wang, J.-L. Sun, *Sci. Rep.* **2015**, *5*, 16563.

[49] C. Cheng, C. Zhu, B. Huang, H. Zhang, H. Zhang, R. Chen, W. Pei, Q. Chen, H. Chen, *Adv. Mater. Technol.* **2019**, *4*, 1800729.

[50] H. Chen, *Adv. Funct. Mater.* **2017**, *27*, 1605654.

[51] A. N. Sokolov, Y. Cao, O. B. Johnson, Z. Bao, *Adv. Funct. Mater.* **2012**, *22*, 175.

[52] S. Kundu, T. L. Kelly, *EcoMat* **2020**, *2*, 12025.

[53] J. A. Steele, H. Jin, I. Dovgaliuk, R. F. Berger, T. Braeckevelt, H. Yuan, C. Martin, E. Solano, K. Lejaeghere, S. M. J. Rogge, C. Notebaert, W. Vandezande, K. P. F. Janssen, B. Goderis, E. Debroye, Y.-K. Wang, Y. Dong, D. Ma, M. Saidaminov, H. Tan, Z. Lu, V. Dyadkin, D. Chernyshov, V. Van Speybroeck, E. H. Sargent, J. Hofkens, M. B. J. Roeffaers, *Science* **2019**, *365*, 679.

[54] Z. Li, T. R. Klein, D. H. Kim, M. Yang, J. J. Berry, M. F. A. M. van Hest, K. Zhu, *Nat. Rev. Mater.* **2018**, *3*, 18017.

[55] J. Rodríguez-Carvajal, *Phys. B* **1993**, *192*, 55.

[56] E. Zolotoyabko, *J. Appl. Crystallogr.* **2009**, *42*, 513.